

# Stability of Texture and Shape of Circular Domains of Langmuir Monolayers

David Pettey and T.C. Lubensky

*Department of Physics and Astronomy, University of Pennsylvania, Philadelphia, PA 19104, USA*

Finite domains of a Langmuir monolayer in a phase with tilted molecules can be modeled by a simple elastic free energy of an  $XY$  order parameter with isotropic and anisotropic line tension terms. The domains can and often do contain nontrivial textures, which in turn influence the shape of the domains. Herein we investigate the properties of a simplified isotropic model with a single elastic constant. For circular domains a first-order phase transition is found between two distinct textures: an exterior defect (or “virtual boojum”) texture, and an interior defect texture. Starting with a circular domain and either of these two textures as a ground state, we find shape instabilities develop that depend on the elastic constants and line tensions in the simplified model. In both cases a necessary but not sufficient condition for the onset of shape instabilities is the possibility for a local negative effective line tension to develop from the anisotropic line tension term.

PACS numbers: 68.18.+p, 68.55.-a, 61.30.Cz, 61.30.Jf, 68.55.Ln, 68.60.-p

## I. INTRODUCTION

The biological importance of thin films of surfactants, such as DPPC (a primary component of human lung surfactant [1]), and other potential commercial applications of self-assembled structures [2] has spurred a resurgence of research in the study of Langmuir films. For the physicist, monolayers of surfactants at the air-water interface provide an interesting  $2D$  system with very rich phase behavior [3,4]. Techniques such as fluorescence microscopy and Brewster angle microscopy allow direct observation of the system as it proceeds through a phase transition. X-ray scattering can also be used. Atomic force microscopy on Langmuir-Blodgett films can provide more detailed information that appears to be consistent with passive observations of the Langmuir film before extraction [5].

Typically, as a film is compressed, it passes from a gas phase (G) to a more condensed liquid expanded phase (LE) to an even more ordered liquid condensed phase (LC) and then, sometimes, into a solid phase before finally becoming a multi-layer film. Experiments have revealed a very complex variety of patterns, shapes, and textures present in the LC/LE and LE/G coexistence regions [6,7]. Upon rapid compression of the film, highly branched structures are often seen. These appear to be the result of diffusion limited aggregation [7], and typically they relax to more regular shapes. More modest compression rates tend to produce a finite number of condensed domains that grow in size, but not number [8], as the film is compressed through a coexistence region. Films composed of enantiomeric surfactants sometimes exhibit domains with a preferred handedness (chirality) to their shape. The handedness alternates with the choice of enantiomer and in racemic mixtures the domains are achiral [6,9,5]. Within domains of the ordered phase, complex structures can sometimes be observed as well [10,11]. The addition of cholesterol to these systems often leads to labyrinthine or striped patterns, and to

spiral domains of a preferred handedness [9].

Molecules in LC phases of Langmuir films either align normal to the air-water interface, or they can tilt relative to the interface [12,13], thereby defining a two-dimensional vector in the plane of the film. In addition some films exhibit hexatic order as well as tilt order [14,15]. Domains of both tilted and non-tilted phases exhibit non-circular shapes [6,11,9,5,16]. Static and dynamic properties of non-tilted domains as well as modulated equilibrium phases are well explained by dipole interactions among the electric dipoles aligned normal to the layers [17–24]. Domain shapes and textures in tilted domains clearly depend on the existence of orientational order in the plane of the film [11,25]. For example, it is difficult to explain chiral shapes that appear in chiral films by a dipole model.

In this paper, we will consider a particularly simple model for tilted domains in which tilt order is described by an isotropic  $XY$ -model and in which coupling between texture and domain shape arises because of an interaction favoring alignment of  $XY$ -vectors at a specific angle with respect to the domain boundaries. This model is clearly oversimplified, but it can explain observed shapes and textures in some systems [11,16,25]. A complete model would allow for different elastic constants for splay and bend distortions and for splay-bend coupling in chiral systems [26] in addition to interactions between electric dipoles with components both parallel and perpendicular to the film. Nonetheless, this simplified isotropic model predicts non-trivial shapes and textures, the full range of which have yet to be analyzed. In spite of its simplicity, it involves highly non-trivial couplings between texture and shape that need to be understood before more realistic models can be studied.

Our model is characterized by three energy parameters; the isotropic elastic constant  $K$  (units of energy), the isotropic line tension  $\gamma$  (units of energy/length) and the line tension  $\mu$  favoring alignment of the  $XY$ -vector  $\hat{\mathbf{m}}$  with the tangent to the domain perimeter  $\hat{\mathbf{t}}$ . We obtain

the following results for this model. For  $\mu/\gamma < 1$ , circular domains are globally stable. Circular domains of radius  $R$  can have two equilibrium textures: one with a strength +1 disclination [27] with core radius  $\xi$  at the center of the domain and one described by a +2 defect (virtual boojum) exterior to the domain [28]. The interior defect texture is favored for large values of  $R/\xi$  whereas the exterior defect texture is favored for large values of  $K/\mu\xi$ . For a circular domain, the exterior defect texture never becomes locally unstable. The interior defect texture does, however, become locally unstable with respect to moving the defect toward the edge of the circle. When  $\mu/\gamma > 1$ , the circular shape and associated textures can become unstable. When the defect is in the interior, the circle can become unstable with respect to  $n$ -fold modulations as the domain radius  $R$  is increased. The value of  $n$  that first becomes unstable depends on  $\mu/\gamma$ . When the defect is outside, the domain becomes unstable with respect to  $n = 2$  distortions first, as  $R$  is increased.

We will proceed with our investigations as follows. We will review the interior and exterior defect textures for a circular domain and then, comparing them, will present a phase diagram for these two textures. Next, we will examine the shape stability by taking an initial configuration consisting of a circular domain and one of the two extremal textures. For each of the two textures we will then allow for perturbations in the shape and texture, calculate an effective free energy dependent only upon the shape, and examine the stability of the circular domain with respect to shape deformations.

## II. THE MODEL AND OUR AIMS

Henceforth we will be concerned only with the following problem. Find the minimum of the free energy [29]

$$F = \frac{1}{2} \int_D K_s [(\nabla \cdot \hat{\mathbf{m}}')^2 + K_b (\nabla \times \hat{\mathbf{m}}')^2] d^2x - \mu' \oint_{\partial D} \hat{\mathbf{m}}' \cdot \hat{\mathbf{t}} ds - \eta' \oint_{\partial D} \hat{\mathbf{m}}' \times \hat{\mathbf{t}} ds + \gamma \oint_{\partial D} ds, \quad (1)$$

over all domains  $D$  with fixed area  $A (= \pi R^2)$ , and over all unit vector fields  $\hat{\mathbf{m}}'$ , for given values of the elastic constants ( $K_s, K_b, \mu', \eta', \gamma$ ).  $K_s$  and  $K_b$  are the usual bend and splay elastic constants,  $\gamma$  is a line tension,  $\hat{\mathbf{t}}$  is the tangent vector to the curve  $\partial D$ , and  $\mu'$  and  $\eta'$  are the coefficients of spontaneous bend and splay, respectively. We have chosen to write the spontaneous bend and splay contributions as line integrals using

$$\begin{aligned} \int_D \nabla \cdot \hat{\mathbf{m}}' d^2x &= \oint_{\partial D} \hat{\mathbf{m}}' \times \hat{\mathbf{t}} ds \\ \int_D \nabla \times \hat{\mathbf{m}}' d^2x &= \oint_{\partial D} \hat{\mathbf{m}}' \cdot \hat{\mathbf{t}} ds. \end{aligned} \quad (2)$$

This allows us to identify  $-\mu' \hat{\mathbf{m}}' \cdot \hat{\mathbf{t}} - \eta' \hat{\mathbf{m}}' \times \hat{\mathbf{t}} + \gamma$  as an effective anisotropic line tension. If  $\gamma < \sqrt{\mu'^2 + \eta'^2}$ , then

choosing  $\hat{\mathbf{m}}'$  to follow  $\hat{\mathbf{t}}$  for a given curve  $\partial D$  will allow the anisotropic line tension to be negative. We will see that within the context of the one-coupling-constant approximation ( $K = K_s = K_b$ ), allowing the effective line tension to become negative will be a necessary condition for instabilities in the shape of a circular domain.

We will now restrict our attention to the one-coupling-constant approximation, simplifying the form of the bulk free energy. Defining  $\Phi'$  via

$$\hat{\mathbf{m}}' = \cos \Phi' \hat{\mathbf{e}}_x + \sin \Phi' \hat{\mathbf{e}}_y, \quad (3)$$

we have

$$\begin{aligned} &\int_D [K_s (\nabla \cdot \hat{\mathbf{m}}')^2 + K_b (\nabla \times \hat{\mathbf{m}}')^2] d^2x \\ &= K \int_D \nabla \Phi' \cdot \nabla \Phi' d^2x. \end{aligned} \quad (4)$$

In appendix B we show that the transformation

$$\begin{aligned} \Phi &= \Phi' - \tan^{-1} \frac{\mu'}{\eta'} - \frac{\pi}{2} \\ \mu &= \sqrt{\mu'^2 + \eta'^2} \\ \hat{\mathbf{m}} &= \cos \Phi \hat{\mathbf{e}}_x + \sin \Phi \hat{\mathbf{e}}_y \end{aligned} \quad (5)$$

simplifies the free energy further:

$$F = \frac{1}{2} K \int_D (\nabla \Phi)^2 d^2x - \mu \oint_{\partial D} \hat{\mathbf{m}} \cdot \hat{\mathbf{t}} ds + \gamma \oint_{\partial D} ds. \quad (6)$$

We could just as easily have transformed away the spontaneous bend term in favor of an effective coefficient for spontaneous splay. Thus, although Eq.(6) is a chiral free energy (the spontaneous bend term is chiral), chirality can only manifest itself through the texture  $\hat{\mathbf{m}}$  and not through the domain shape  $D$  ( $D$  is invariant under the transformation, see App. B).

To make contact with previous work [16] we note that we could have written our surface term in the form

$$\oint_{\partial D} \sigma(\theta - \Phi) ds, \quad (7)$$

where the outward normal to the boundary is given by

$$\hat{\mathbf{n}} = \cos \theta \hat{\mathbf{e}}_x + \sin \theta \hat{\mathbf{e}}_y, \quad (8)$$

and

$$\sigma(x) = \gamma + \sum_{n=1}^{\infty} (a_n \cos nx + b_n \sin nx). \quad (9)$$

Taking  $b_1 = -\mu$  with all other  $a_n$ 's and  $b_n$ 's set to zero will recover our effective line tension

$$\gamma \oint_{\partial D} ds - \mu \oint_{\partial D} \hat{\mathbf{m}} \cdot \hat{\mathbf{t}} ds. \quad (10)$$

Similarly a nonzero  $a_1$  will produce a spontaneous splay contribution. The transformation (5), in this language,

allows the elimination of the  $a_1$  ( $b_1$ ) term in favor of a new effective  $b'_1$  ( $a'_1$ ).

Rudnick and Bruinsma [16] have demonstrated that a nonzero  $a_2$ , in addition to a nonzero  $a_1$ , leads to non-circular shapes and nontrivial textures in agreement with some experiments [25]. However, Rivière and Meunier [11] can account for these same shapes and textures without a nonzero  $a_2$  by incorporating the apparent anisotropy between  $K_s$  and  $K_b$ . We will show that even with  $K_s = K_b$  and  $a_2 = 0$  [as in Eq. (6)] shape instabilities *still* exist when  $\gamma < \mu$ , that is, once a negative effective line tension is allowed.

To see that instabilities should arise, we first identify

$$\begin{aligned} A_b &= \frac{K}{\mu R} \\ A_s &= \frac{\mu}{\gamma} - 1 \end{aligned} \quad (11)$$

as two independent dimensionless parameters.  $A_b$  is a measure of the competition between the bulk energy and the anisotropic piece of the line tension. For a given  $\partial D$ ,  $A_b$  will determine the preferred texture.  $A_s$  measures the relative strength of the anisotropic and isotropic contributions to the effective line tension. When  $A_s > 0$ , the effective line tension can be negative.

When  $A_b \rightarrow \infty$  we can assume that  $K \rightarrow \infty$  and hence that  $\hat{\mathbf{m}}$  will be constrained to be a constant. Thus, without loss of generality, we can assume that  $\hat{\mathbf{m}} = \hat{\mathbf{e}}_y$ . This form for  $\hat{\mathbf{m}}$  yields

$$\oint_{\partial D} \hat{\mathbf{m}} \cdot \hat{\mathbf{t}} ds = 0 \quad (12)$$

for all  $\partial D$ , and as such the value of  $\mu$  is irrelevant. In fact, the free energy is simply

$$F = \gamma \oint_{\partial D} ds. \quad (13)$$

For fixed area,  $A$ , the preferred shape will simply be a circle.

In contrast, when  $A_b \rightarrow 0$  we assume  $K \rightarrow 0$  and thus  $\hat{\mathbf{m}}$  can take any form it chooses in the bulk. In particular, we can always choose  $\hat{\mathbf{m}}$  such that  $\hat{\mathbf{m}} \cdot \hat{\mathbf{t}} = 1$  at all points on the curve, for any curve  $\partial D$ . Thus now our free energy becomes

$$F = (\gamma - \mu) \oint_{\partial D} ds. \quad (14)$$

If  $\gamma > \mu$  then certainly we again have a circle as the preferred shape. But if  $\gamma < \mu$  then the domain attempts to maximize the length of its boundary,  $\partial D$ . This results in pathologically distorted shapes, or unbounded domains. Thus, when  $\gamma < \mu$  we anticipate that for large  $A_b$  the domain shapes will be circular, but for small  $A_b$  the shapes will begin to distort. However, when  $\gamma > \mu$  it would not be at all surprising to find that the circular domains are preferred for all values of  $A_b$ .

We are now ready to begin our search for optimal shape and texture configurations. Although we will restrict our attention to the one-coupling-constant approximation, which provides us with a particularly simple bulk Euler-Lagrange equation

$$\nabla^2 \Phi = 0, \quad (15)$$

it is still not a trivial task to find the optimum  $\Phi$  for a generic domain  $D$ . We will approach the problem as follows. Noting that experimentally the domains appear to be circular for small  $A$ , we will first fix the domain shape to be a circle and try to find the optimum  $\Phi$ . This is tantamount to assuming that  $\gamma$  is infinite. Having found the optimal texture for a circular domain, we will then allow the shape and texture to deform. The next section will deal with the task of finding the optimal texture for a circular domain and the succeeding section will deal with instabilities in the shape of the domain.

### III. THE OPTIMAL TEXTURE FOR A CIRCULAR DOMAIN

The main question to address here is whether the domain should contain a topological defect. In experiments by Rivière and Meunier [11] the domain clearly does not contain a defect and has the “virtual boojum” texture previously described by Sethna [28]. However in [10] Qiu *et al.* observed a star defect inside the domain, which indicates that it may be possible to have an isolated +1 defect inside a domain when hexatic order is not present (as the hexatic order is lost the arms of the star defect retract and one is left with a simple +1 defect [30–32]). Also, in thin films of smectic-C liquid crystals, which can be approximately modeled by the same free energy, isolated +1 defects are often observed [27].

Fixing the domain to be a disk, the isotropic line tension term will be irrelevant to this discussion since it is unaffected by changes in texture alone. The anisotropic piece of the boundary energy, however, favors having  $\hat{\mathbf{m}}$  parallel to the tangent to the boundary and thus prefers having either a +1 defect inside the domain or a +2 defect on the boundary (sometimes referred to as a boojum). The bulk portion of the free energy clearly prefers that  $\hat{\mathbf{m}}$  simply be uniform within the domain. Thus, whether it is preferable to have a defect inside the domain or not depends upon the competition between the bulk elastic energy and the anisotropic line tension, as well as upon the energy cost required to nucleate a melted defect core.

In this section we will first review the virtual boojum texture, which is an extremal texture for the case where there is no defect inside the disk [16]. In fact, in section IV A we will show that this is a locally minimal texture with respect to our free energy. Next we will consider textures associated with the defect inside the domain. We will note that the texture for an isolated +1 defect at the center of the domain is extremal and for

$A_b < 1$  it is a local minimum as well. We will investigate a class of ansatz textures consisting of an isolated +1 defect located anywhere within the domain. We will find that within this restricted class of textures, there is a first-order transition between the texture with the defect at the center of the disk and a texture with the defect close to the boundary. Thus, we find that not only is the texture of the defect at the center of the disk unstable for  $A_b > 1$  but that it also fails to be a global minimum for even smaller values of  $A_b$  within the class of textures with an enclosed defect. In contrast, the virtual boojum texture is a local minimum for all values of  $A_b$ .

Finally, we compare the virtual boojum texture with the texture of the defect at the center of the disk. We find a first-order transition between these two textures which is most easily described by the dimensionless parameters  $c = K/2\mu\xi$ ,  $x = R/\xi$ , and  $g$ , where  $\xi$  is the coherence length and  $g$  is a phenomenological parameter associated with the energy cost of a defect core (in our calculations we will take  $g = 1$ ).

### A. Virtual Boojum

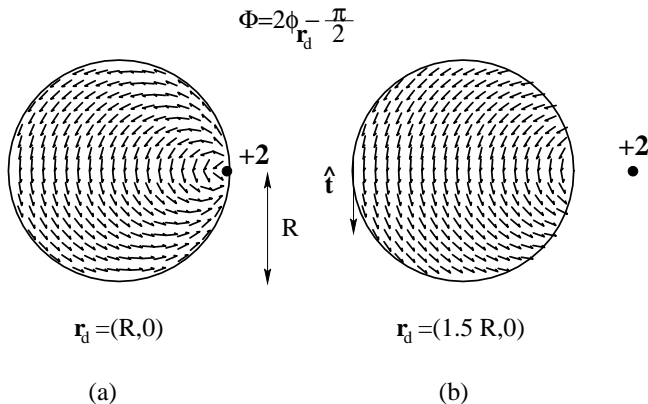


FIG. 1. Textures arising from a single +2 defect. The constant term in  $\Phi$  has been chosen to make  $\hat{\mathbf{m}}$  as close to  $\hat{\mathbf{t}}$  (the tangent vector) as possible. With the defect at the boundary (a) we have  $\hat{\mathbf{m}} \cdot \hat{\mathbf{t}} = 1$  but we also have very large gradients in  $\hat{\mathbf{m}}$  near the defect. In (b) these large gradients have been expelled along with the defect but now we no longer have  $\hat{\mathbf{m}} \cdot \hat{\mathbf{t}} = 1$ . The competition between the ideal boundary ( $\hat{\mathbf{m}} \cdot \hat{\mathbf{t}} = 1$ ) and bulk ( $\partial_i \hat{\mathbf{m}} = 0$ ) conditions leads to a preferred separation distance between the domain and the defect.

Let us now recall the virtual boojum texture [28]. This is simply the texture produced by a single +2 defect sitting outside the disk (Fig. 1). With the following notation,

$$\begin{aligned} \mathbf{r} &= (r \cos \phi, r \sin \phi) = (x, y) \\ z &= x + iy \\ \phi_{\mathbf{r}_d}(\mathbf{r}) &= \text{Im}(\log |z - z_d|) = \tan^{-1} \left( \frac{y - y_d}{x - x_d} \right) \end{aligned} \quad (16)$$

the field for a +2 defect located at  $\mathbf{r}_d = (r_d \cos \phi_d, r_d \sin \phi_d) = (x_d, y_d)$  is just

$$\Phi = 2\phi_{\mathbf{r}_d}(\mathbf{r}) + C. \quad (17)$$

Clearly the texture satisfies the bulk Euler-Lagrange equation,  $\nabla^2 \Phi = 0$ . Furthermore, this collection of textures (one for each  $\mathbf{r}_d$  and  $C$ ) smoothly varies in its extremes from the uniform texture ( $\mathbf{r}_d \rightarrow \infty$ ,  $\hat{\mathbf{m}} \rightarrow \text{constant}$ ), which is preferred when  $\mu = 0$ , to a texture where  $\hat{\mathbf{m}} \cdot \hat{\mathbf{t}} = 1$  ( $r_d = R$ ), which is preferred when  $\mu \rightarrow \infty$ .

Taking the domain to be a disk of radius  $R$  centered at the origin we then find that Eq. (6) yields

$$\begin{aligned} F &= -2\pi K \log \left( 1 - \left( \frac{R}{r_d} \right)^2 \right) + 2\pi \frac{\mu}{r_d} R^2 \sin(C + \phi_d) \\ &\quad + 2\pi\gamma R, \end{aligned} \quad (18)$$

where we have assumed that the defect is outside the disk at least a core radius,  $\xi$ , away from the boundary ( $r_d > R + \xi$ ). Minimizing over  $C$  we find the preferred value of  $C$  to be,

$$C^0 = -\frac{\pi}{2} - \phi_d. \quad (19)$$

Without loss of generality we can take  $\phi_d = 0$ , and finally write the energy for a +2 defect outside the disk, on the positive  $x$ -axis as,

$$F_{+2} = -2\pi K \log \left( 1 - \left( \frac{R}{r_d} \right)^2 \right) - 2\pi \frac{\mu}{r_d} R^2 + 2\pi\gamma R. \quad (20)$$

For a given value of the dimensionless quantity

$$A_b = \frac{K}{\mu R} \quad (21)$$

there is a preferred stable minimum value [28,16] for  $r_d$  given by

$$r_d^0 = R(A_b + \sqrt{1 + A_b^2}). \quad (22)$$

Furthermore, we see that using this value of  $r_d$  in our  $F_{+2}$  above yields  $F_{+2}(r_d^0) < 2\pi\gamma R$ , revealing that this texture is preferred over the uniform texture for all values of  $A_b$ .

Rudnick and Bruinsma [16] have shown that this texture with the defect at  $r_d^0$  is in fact extremal. We will further show that this texture is indeed a local minimum when we investigate shape instabilities in section IV.

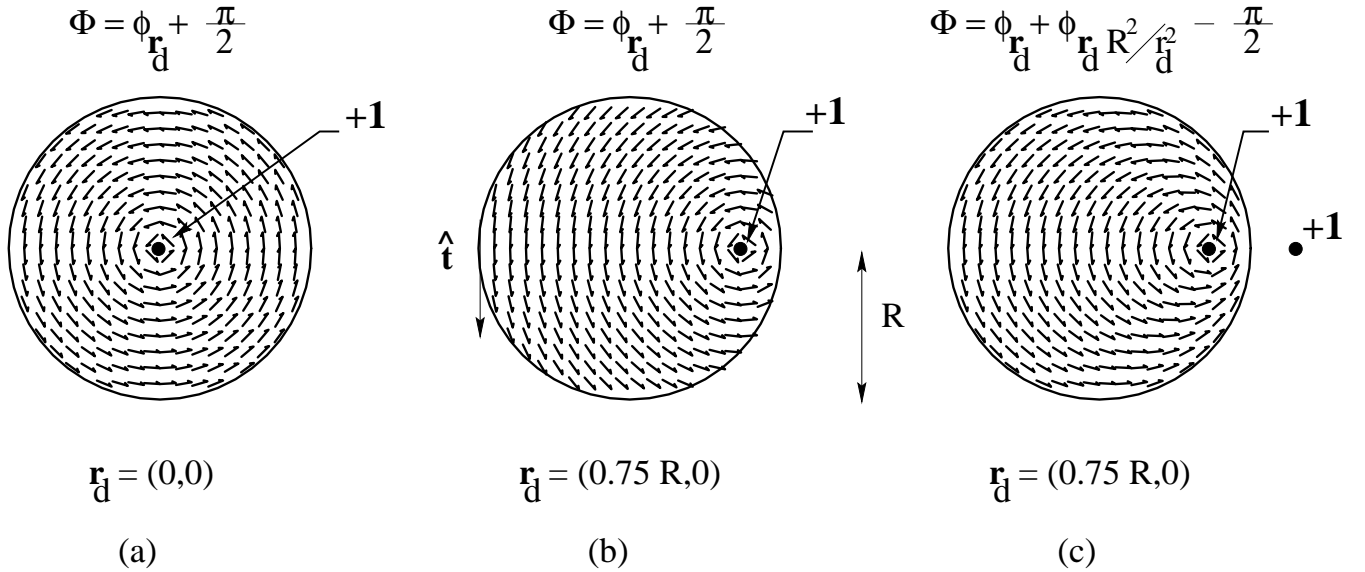


FIG. 2. Texture arising from a +1 defect inside the disk. The textures in (a) and (b) arise solely from the interior defect, whereas the texture in (c) includes the effects of an image defect outside the domain. Notice that in (a) and (b) we have  $\hat{\mathbf{m}} \cdot \hat{\mathbf{t}} = 1$  whereas in (b) we do not.

### B. Defect Inside

Here we will look at the class of ansatz textures

$$\Phi = \phi_{r_d}(\mathbf{r}) + \frac{\pi}{2} \quad (23)$$

where we assume  $r_d < R - \xi$  (i.e. the defect is inside the disk and at least a core radius,  $\xi$ , away from the boundary). Without loss of generality we take  $\phi_d = 0$  and accordingly we have already chosen the constant term to be the optimal value. Again, clearly, all such textures satisfy the bulk Euler-Lagrange equation,  $\nabla^2 \Phi = 0$ , within the domain, except at the position of the defect. We note that when  $r_d = 0$ ,  $\hat{\mathbf{m}}$  is parallel to the tangent to the boundary (Fig. 2).

Applying Eq. (6) we find that the energy of this texture is

$$F_{+1} = \pi K \log\left(\frac{R}{\xi}\right) + \frac{\pi K}{2} \log\left(1 - \frac{r_d^2}{R^2}\right) - 4\mu R E\left(\frac{r_d}{R}\right) + 2\pi\gamma R + \epsilon_{\text{core}}, \quad (24)$$

where we have introduced a term for the core energy,  $\epsilon_{\text{core}}$ .  $E(x)$  is the complete elliptic integral of the second kind,

$$E(x) = \int_0^{\frac{\pi}{2}} \sqrt{1 - x^2 \sin^2 \phi} d\phi. \quad (25)$$

We will see in section IV, when we investigate changes in shape and texture, that when  $r_d = 0$  and  $A_b < 1$  this texture is a local minimum with respect to all variations in the texture (not just variations within this ansatz class). However, we find that  $r_d = 0$  and  $A_b < 1$  does not always yield a global minimum even within this class (23).

The free energy (24) has an interesting behavior as we vary  $r_d$ . As we move the defect off center, there is an energy increase from the boundary term but a decrease in energy from the bulk term. The two contributions have quite different functional forms, and we find that, depending upon the value of  $A_b = K/\mu R$ , it may be preferable either to keep the defect at the origin or to allow it to migrate towards the boundary. Maintaining  $0 < r_d < R - \xi$  we find the following behavior of (24) within this class of textures,

$$\begin{aligned} A_b < 0.23 &\rightarrow r_d = 0 \text{ is a global minimum} \\ A_b < 1 &\rightarrow r_d = 0 \text{ is a local minimum} \\ A_b > 1 &\rightarrow r_d = 0 \text{ is a local maximum.} \end{aligned} \quad (26)$$

This behavior is summarized in Fig. 3. We see that within this class of textures there is a first-order transition in the position of the defect as we change  $A_b$ . When  $r_d = 0$  becomes the global minimum, it may in fact already be the case that the energy barrier that must be overcome in order for the defect to migrate from the boundary to the origin may already be too high for this to be a physically probable event. Note that we have limited our attention only to a particular subset of potential textures and this barrier may not remain if we were to consider all possible textures. However, we are aware of no experimental observations corresponding to a single +1 defect near the boundary of the domain. Thus, overall we conclude that when a defect is present within the domain it is very likely to be at the origin in a stable local minimum.

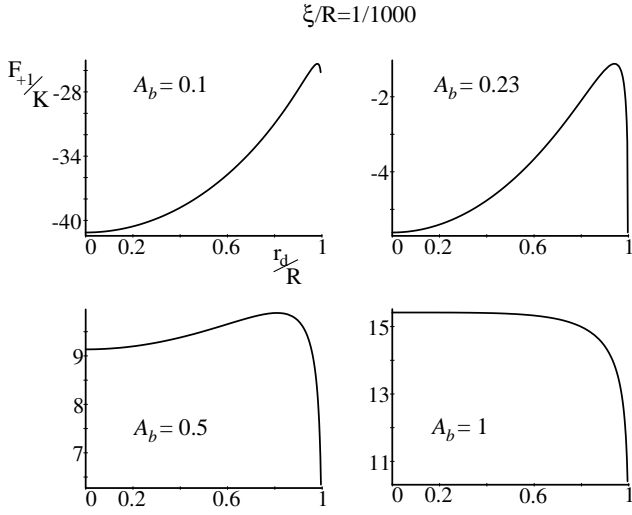


FIG. 3. Plots of  $F_{+1}/K$  vs  $r_d/R$  for a disk of radius  $R$  for several values of  $A_b$ . We have taken  $\xi/R = 1/1000$  and have restricted  $r_d/R$  to be less than  $1 - 1/1000$ , so that the entire defect core is within the disk. We have also not included the core energy  $\epsilon_{core}$  or the isotropic line tension  $2\pi\gamma\mu R$  in  $F_{+1}$ , which here are merely uninteresting constants. Note that  $r_d = 0$  is a local minimum whenever  $A_b < 1$  and  $r_d \approx R$  appears to be a local minimum for all of the plots. When  $A_b < 0.23$  then  $r_d = 0$  appears to be the true minimum. Notice that the barrier separating the two minima is approximately  $4K$  at  $A_b = 0.23$ .

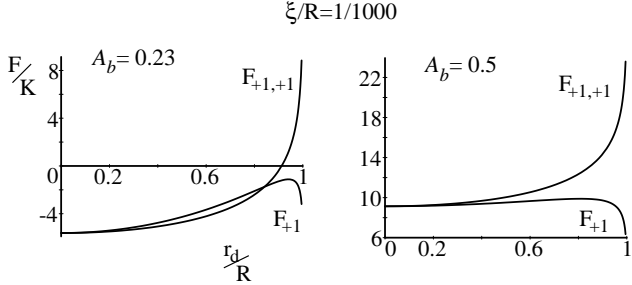


FIG. 4. A comparison of the energy of an isolated +1 defect in the disk,  $F_{+1}$  with the energy of a +1 defect inside along with an image defect outside enforcing strong pinning boundary conditions ( $\hat{\mathbf{m}} \cdot \hat{\mathbf{t}} = 1$ ),  $F_{+1,+1}$ . Note that the energies are equal at  $R_d = 0$ . At the boundary of the disk ( $r_d = R - \xi$ )  $F_{+1}$  is always lower. Even though for some intermediate values of  $r_d$   $F_{+1,+1}$  is smaller than  $F_{+1}$  it is never substantially smaller.

We note that one can also consider the texture,

$$\Phi = \phi_{\mathbf{r}_d}(\mathbf{r}) + \phi_{\mathbf{r}_d R^2/r_d^2}(\mathbf{r}) - \frac{\pi}{2}, \quad (27)$$

which corresponds to a defect inside the domain along with an image defect outside the domain which enforces strong pinning boundary conditions,  $\hat{\mathbf{m}} \cdot \hat{\mathbf{t}} = 1$  (where again we take  $\phi_d = 0$ ). Within this class textures the defect always prefers to be at the origin, and when  $A_b > 0.23$  this texture provides at best a modest improvement

over (23) and never offers a lower global minimum (Fig. 4). Of course, when  $r_d = 0$  this texture is the same as (23) with  $r_d = 0$ .

### C. Which texture wins?

We have presented two textures which are local minima of the free energy (6). For the +2 exterior defect texture we found a local minimum for all values of  $A_b$  ((17) with  $\phi_d = 0$  and  $r_d = r_d^0$  (22)). For the +1 interior defect texture we found a local minimum only for  $A_b < 1$  ((23) with  $\mathbf{r}_d = 0$ ). Furthermore, we found that this local minimum was not the global minimum even within the class of ansatz textures (23). Here we will compare the energies of the two locally minimal textures to see which is favored.

For small  $R$  the bulk energy dominates the boundary energy and we expect the uniform texture to win. Since the +2 defect texture produces the uniform texture in the limit  $A_b \rightarrow \infty$  ( $R \rightarrow 0$ ) we anticipate that for small  $R$  this texture will be favored. For large  $R$  ( $A_b \rightarrow 0$ ) both textures satisfy strong pinning boundary conditions and thus have equal contributions from the surface energy. However, the bulk energy cost of the exterior defect texture is greater than that of the interior defect texture. This can be understood qualitatively by recalling that the bulk energy cost of a defect of charge  $q$  centered in a disk of radius  $R$  is  $\pi K q^2 \log(R/\xi)$  [27]. In the limit of large  $R$  the +1 defect energy will be  $\pi K \log(R/\xi)$  whereas the +2 defect energy will be  $\approx (1/2)2^2 \pi K \log(R/\xi)$ . The factor of  $(1/2)$  arises because the +2 defect is at the boundary of the disk, not the center.

Thus, we will find a first-order transition between the two textures. In discussing this transition we find it more convenient to refer to the dimensionless quantities

$$c = \frac{K}{2\mu\xi} \quad \text{and} \quad x = \frac{R}{\xi} \quad (28)$$

rather than  $A_b$  and  $R/\xi$ . Assuming that  $R > \xi$  we find that when  $c < 0.85$  the interior defect solution is favored. For larger values of  $c$ , there is a critical radius,  $R_{crit}(c)$ , above which the interior defect texture is favored and below which the exterior texture is favored. Thus  $R_{crit}(c)$  defines the first-order phase boundary  $\Gamma$  in Fig. 5.

Note in Fig. 5 that we have also included the curve  $A_b = 1$  which is the boundary at which the interior defect solution becomes unstable. There is a large separation between this boundary and the transition line  $\Gamma$ . In the region above the  $A_b = 1$  curve both textures are local minima and hence a physical system may well find itself trapped in a meta-stable local minimum when  $A_b < 1$ . Furthermore, in section III B we found some circumstantial evidence suggesting that the barrier preventing the expulsion of the interior defect may be quite large for physically realisable values of  $A_b$  (Fig. 3). Indeed in an experiment [25] that apparently has the exterior defect

texture, taking  $\xi \approx 100\text{nm}$  yields  $c \approx 2$ . However, the radii of the domains appears to be as large as  $10\mu\text{m}$ , which is much larger than the critical radius for  $c = 2$  ( $R_{\text{crit}}(2) \approx 2\mu\text{m}$ ), suggesting that it may be the case that this texture is a meta-stable equilibrium state.

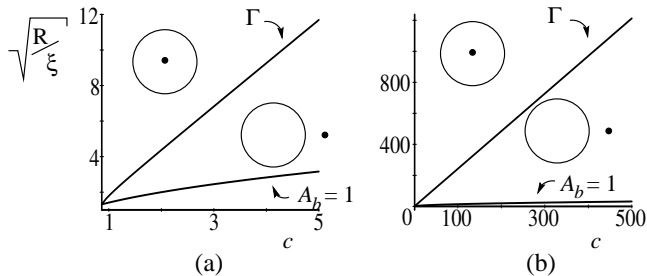


FIG. 5. The two figures display at different scales the phase diagram for the +1 defect at the center of the disk versus the exterior +2 defect texture. The curve  $\Gamma$  is  $R = R_{\text{crit}}(c)$  where  $R_{\text{crit}}(c)$  is the critical radius for a given value of  $c$  as discussed section III C. The lower curve is  $A_b = 1$ . To the left and above  $\Gamma$  the interior defect texture is favored, below the exterior defect is favored. However, the interior defect texture is a local minimum in the region above the curve  $A_b = 1$  and the exterior region is a local minimum throughout the region.

To identify the transition we simply compare  $F_{+1}$  and  $F_{+2}$ . Taking  $\epsilon_{\text{core}} = \pi K$  and noting that  $A_b = 2c/x$  we can write (24) as

$$F_{+1} = \pi\mu R \left( \frac{2c}{x} \log x - 2 + \frac{2c}{x} \right) + 2\pi\gamma R. \quad (29)$$

With  $\phi_d = 0$  and  $r_d = r_d^0$  we can also write (20) as

$$F_{+2} = \pi\mu R \left( -\frac{4c}{x} \log \left( 1 - h^2 \left( \frac{2c}{x} \right) \right) - 2h \left( \frac{2c}{x} \right) \right) + 2\pi\gamma R. \quad (30)$$

where

$$h(y) = \frac{1}{y + \sqrt{1 + y^2}}. \quad (31)$$

Examining  $F_{+1} - F_{+2}$  we find that when  $c < c^* \approx 0.85$  the interior defect solution is preferred for all values of  $R$  (or equivalently all values of  $x$  since we are assuming that  $\xi$  is constant). For larger values of  $c$  we find that there is a critical value of  $R$ ,  $R_{\text{crit}}(c)$ , below which the exterior defect solution is favored (Fig. 5).

#### IV. SHAPE CHANGES

For circular domains we have found two distinct textures which are local minima of the free energy (this will be demonstrated soon). Now for each of these textures we would like to know if the configuration  $(D, \Phi_0)$ , where

$D$  is a disk and  $\Phi_0$  is either of the two textures, is a minimum with respect to changes in shape and texture. We will find in each case that although the texture is stable when the shape is fixed, the configuration (shape and texture) is unstable for certain values of  $A_b$  and  $A_s$ . We will see that when  $\mu > \gamma$  ( $A_s > 0$ ) instabilities will begin to arise.

To examine the stability of the configurations we need to introduce perturbations in the shape and texture. To this end we take  $D$  to be the region bounded by the curve, given in polar coordinates by

$$\begin{aligned} r(\phi) &= R_0 + \sum_{n \in \mathbb{Z} - \{0\}} \rho_n e^{in\phi} \\ &= R_0 + \sum_{n \in \mathbb{Z}^+} (a_n \cos n\phi + b_n \sin n\phi), \end{aligned} \quad (32)$$

where

$$\rho_n = \rho_{-n}^* = \frac{1}{2}(a_n - ib_n) \quad (33)$$

and  $R$  is defined by

$$\begin{aligned} R_0 &= R \left( 1 - \sum_{n \in \mathbb{Z} - \{0\}} \frac{\rho_n \rho_{-n}}{R^2} \right)^{\frac{1}{2}} \\ &= R \left( 1 - \frac{1}{2} \sum_{n \in \mathbb{Z}^+} \frac{a_n^2 + b_n^2}{R^2} \right)^{\frac{1}{2}}. \end{aligned} \quad (34)$$

With this parameterization the area of the domain is simply

$$A = \pi R^2. \quad (35)$$

Thus keeping  $R$  fixed keeps the area constant. Note that we have included the  $n = 1$  terms in (32). Although these modes can usually be ignored as being just translations of  $D$  (to lowest order in the Fourier coefficients), here the texture distinguishes a particular origin for the coordinate system and as such translations of  $D$  are associated with nontrivial changes in the configuration (see App. A).

To allow for perturbations in the texture we will take

$$\Phi(\mathbf{r}) = \Phi_0(\mathbf{r}) + \sum_{n \in \mathbb{Z} - \{0\}} r^{|n|} P_n e^{in\phi} \quad \text{with} \quad P_n = P_{-n}^*, \quad (36)$$

where  $\Phi_0(\mathbf{r})$  is one of the two textures found in section III ((17) and (23)) and the perturbation is the most general nonsingular addition allowed by the Euler-Lagrange equation  $\nabla^2 \Phi = 0$ . Taking  $O(P_n) = O(\rho_n) = O(\epsilon)$  we will proceed to calculate  $F$  to order  $\epsilon^2$ . This will provide us with an approximation to

$$F(\boldsymbol{\rho}, \mathbf{P}, K, \gamma, \mu, R), \quad (37)$$

where

$$\begin{aligned}\boldsymbol{\rho} &= (\rho_1, \rho_{-1}, \rho_2, \rho_{-2}, \dots) \quad \text{and} \\ \mathbf{P} &= (P_1, P_{-1}, P_2, P_{-2}, \dots).\end{aligned}\quad (38)$$

Minimizing this over  $\mathbf{P}$  we will obtain the effective free energy,

$$F_{\text{eff}}(\boldsymbol{\rho}, K, \gamma, \mu, R), \quad (39)$$

as a function of the elastic constants, the radius, and the shape perturbation parameters correct to  $O(\epsilon^2)$ .

In both cases we find that  $F_{\text{eff}}$  contains no terms of  $O(\epsilon)$ , that is no terms linear in  $\rho_n$ , demonstrating that the configurations are extremal. We also find that when  $\mu > \gamma$  shape instabilities will be present for certain values of  $A_b$  and  $A_s$ . In fact, for any given  $A_s > 0$  we find that instabilities arise for sufficiently small  $A_b$ 's.

Ideally we would like to calculate  $F_{\text{eff}}$  correct to all orders in  $\{\rho_n\}$ . Then minimization of  $F_{\text{eff}}$  over the  $\rho_n$ 's would yield distorted equilibrium shapes. Unfortunately this is a prohibitively difficult task. Alternatively, we would like to calculate  $F_{\text{eff}}$  to high enough order in  $\epsilon$  such that the effective energy is bounded below. This would provide approximations to the equilibrium values of the  $\rho_n$ 's, and thus approximations to distorted equilibrium domain shapes. Calculating  $F_{\text{eff}}$  to  $O(\epsilon^4)$ , while difficult but not impossible, is not sufficient. This appears to be due to the form of  $\gamma \oint_{\partial D} ds$  as a function of the  $\rho_n$ 's. Although this isotropic line tension term should be stabilizing the boundary against deformations, the fourth order coefficients are negative and as such they lead to  $F_{\text{eff}}$  being unbounded below at  $O(\epsilon^4)$ . Because of extensive mode coupling and the exponential increase in the number of terms in  $F_{\text{eff}}$  we have not proceeded to  $O(\epsilon^6)$ .

### A. The exterior defect

We will now apply the outlined procedure to the case of the exterior defect. We take  $D$  as in (32) and we take

$$\Phi_0 = 2\phi_{\mathbf{r}_d^0}(\mathbf{r}) - \frac{\pi}{2}, \quad (40)$$

the preferred texture for a disk, as found in section III A. We will not allow  $\mathbf{r}_d^0$  to vary, nor will we allow for variations in the constant term ( $C = -\pi/2$ ). Allowing  $\mathbf{r}_d^0$  to vary would present us with a redundancy in the definition of  $\Phi$  (36). Namely, changes in  $\mathbf{r}_d^0$  are already accounted for by the  $P_n$ 's in (36). If we wished to have

$$\Phi = 2\phi_{\mathbf{r}_d} - \frac{\pi}{2} \quad (41)$$

where  $\mathbf{r}_d \neq \mathbf{r}_d^0$  this could be achieved by an appropriate choice of the  $P_n$ 's in (36) since the perturbative terms form a complete set of solutions to Laplace's equation in the disk.

Noting the  $\sin(C + \phi_d)$  term in (18), we see that rotating the defect about the center of the disk and simultaneously adjusting  $C$  to maintain  $C + \phi_d = -\pi/2$  costs no energy. As we have just noted, an appropriate choice of the  $P_n$ 's will produce this rotation, and thus if  $C$  were allowed to vary, we would discover this Goldstone mode eventually. By fixing  $C$  to be  $-\pi/2$  we freeze out this mode. Experimental evidence suggests that this is the appropriate course to take. The texture associated with a +2 virtual defect has been observed [11,25], demonstrating that on the time scale of the observations the virtual defect does not freely rotate about the domain. If the defect did execute such a motion, then the time averaged texture would appear as the trivial texture. Though a careful consideration of the dynamics might be in order, in this paper we will not concern ourselves further with the origin of the observed angular stability of the virtual defect.

We find it more convenient now to use the real rather than the complex fourier coefficients in calculating  $F$ :

$$\begin{aligned}A_n &= 2\text{Re}[P_n] \quad B_n = 2\text{Im}[P_n] \quad P_n = \frac{1}{2}(A_n + iB_n) \\ a_n &= 2\text{Re}[\rho_n] \quad b_n = 2\text{Im}[\rho_n] \quad \rho_n = \frac{1}{2}(a_n + ib_n).\end{aligned}\quad (42)$$

Thus, now  $\mathbf{A} = (A_1, A_2, \dots)$  and  $\mathbf{B} = (B_1, B_2, \dots)$  describe texture changes whereas  $\mathbf{a} = (a_1, a_2, \dots)$  and  $\mathbf{b} = (b_1, b_2, \dots)$  describe shape changes. Taking  $K = 1$  and  $R = 1$  to set our energy and length scales, and performing a plethora of contour integrals we eventually find

$$\begin{aligned}F(\mathbf{A}, \mathbf{B}, \mathbf{a}, \mathbf{b}, A_b, A_s) &= \langle \mathbf{A} | H_{AA} | \mathbf{A} \rangle + \langle \mathbf{B} | H_{BB} | \mathbf{B} \rangle \\ &+ \langle \mathbf{a} | H_{aa} | \mathbf{a} \rangle + \langle \mathbf{b} | H_{bb} | \mathbf{b} \rangle \\ &+ \langle \mathbf{A} | U_{Ab} | \mathbf{b} \rangle + \langle \mathbf{B} | U_{Ba} | \mathbf{a} \rangle \\ &+ F_{+2},\end{aligned}\quad (43)$$

where

$$\begin{aligned}(H_{AA})_{n,m} &= (H_{BB})_{n,m} = \\ &= \frac{-\mu\pi}{4} \left( \frac{1}{(r_d^0)^{m+n-1}} - \frac{1}{(r_d^0)^{m+n+1}} \right) \\ &- \frac{\mu\pi}{4} \left( \frac{1 - \delta_{m,n}}{(r_d^0)^{|m-n|-1}} - \frac{1 - \delta_{m,n}}{(r_d^0)^{|m-n|+1}} \right) \\ &+ \frac{\mu\pi}{2r_d^0} \delta_{m,n} + 2\pi m \delta_{m,n},\end{aligned}\quad (44)$$

$$\begin{aligned}(U_{Ab})_{n,m} &= \\ &= \frac{\mu\pi}{r_d^0} \left( \frac{1}{(r_d^0)^{m+n}} + (-1)^{n-m+1} 2 \frac{1 - \delta_{m,n}}{(r_d^0)^{|n-m|}} - 2m \delta_{m,n} \right),\end{aligned}\quad (45)$$

$$\begin{aligned}(U_{Ba})_{n,m} &= \\ &= \frac{\mu\pi}{r_d^0} \left( \frac{1}{(r_d^0)^{m+n}} + (-1)^{n-m} 2 \frac{1 - \delta_{m,n}}{(r_d^0)^{|n-m|}} + 2m \delta_{m,n} \right),\end{aligned}\quad (46)$$

and

$$(H_{aa})_{n,m} = \frac{1}{2}(h(n,m) + h(n,-m)) + \frac{1}{2}\pi\gamma(n^2 - 1)\delta_{m,n}, \quad (47)$$

$$(H_{bb})_{n,m} = \frac{1}{2}(-h(n,m) + h(n,-m)) + \frac{1}{2}\pi\gamma(n^2 - 1)\delta_{m,n}, \quad (48)$$

where

$$\begin{aligned} h(n,m) &= \pi\mu(1 - \delta_{m,-n}) \\ &\times \left[ \frac{|m+n|-2}{2} \left( \frac{|m+n|+1}{(r_d^0)^{|m+n|+1}} - \frac{|m+n|-1}{(r_d^0)^{|m+n|-1}} \right) \right. \\ &+ \left. \frac{(|m+n|-2)(|m+n|-1)}{2(r_d^0)^{|m+n|-1}} - \frac{|m+n|(|m+n|+1)}{2(r_d^0)^{|m+n|+1}} \right] \\ &- \frac{2\pi}{(r_d^0)^2 - 1} \delta_{m,-n} \\ &+ \frac{2\pi}{(r_d^0)^{|m+n|}} \left( \frac{|m+n|+1}{(r_d^0)^2 - 1} + \frac{2}{((r_d^0)^2 - 1)^2} \right). \end{aligned} \quad (49)$$

For convenience we have chosen to leave the above in terms of  $\mu$ ,  $\gamma$  and  $r_d^0$ . With  $K = 1$  and  $R = 1$  we have,

$$\begin{aligned} \mu &= \frac{1}{A_b} \\ r_d^0 &= A_b + \sqrt{A_b^2 + 1} \\ \gamma &= \frac{\mu}{A_s + 1} = \frac{A_b}{A_s + 1}. \end{aligned} \quad (50)$$

Note the absence of any terms linear in  $\{\mathbf{A}, \mathbf{B}, \mathbf{a}, \mathbf{b}\}$  in (43). This confirms that the unperturbed configuration is an extremum. Furthermore,  $H_{AA}, H_{BB}, H_{aa}$  and  $H_{bb}$  are all positive definite. Thus the unperturbed configuration is actually a minimum with respect to changes in either texture or shape alone. Any instabilities must therefore arise as a result of the couplings,  $U_{Ab}$  and  $U_{Ba}$ , between shape and texture.

Before minimizing over  $\mathbf{A}$  and  $\mathbf{B}$  to find  $F_{\text{eff}}$  we note that two Goldstone modes are still present. A simultaneous translation of the domain and the defect will not change the energy,  $F$ . This implies the existence of 2 zero eigenvalues in  $F$ , one for horizontal and one for vertical translations. These translations are achieved through appropriate choices for  $\mathbf{A}, \mathbf{B}, \mathbf{a}$  and  $\mathbf{b}$ . For example, the infinitesimal translation  $\epsilon \hat{\mathbf{e}}_x$  is achieved by taking

$$\begin{aligned} a_1 &= \epsilon \\ B_n &= -\frac{2\epsilon}{(r_d^0)^{n+1}}. \end{aligned} \quad (51)$$

The two Goldstone modes should be present in  $F_{\text{eff}}$  and we will use their existence as a check on our calculations.

Symbolically, calculating  $F_{\text{eff}}$  is straightforward,

$$F_{\text{eff}}(\mathbf{a}, \mathbf{b}) = \langle \mathbf{a} | H_{aa} + Q_{aa} | \mathbf{a} \rangle + \langle \mathbf{b} | H_{bb} + Q_{bb} | \mathbf{b} \rangle, \quad (52)$$

where

$$\begin{aligned} Q_{aa} &= -\frac{1}{4}U_{Ba}^T H_{BB}^{-1} U_{Ba} \\ Q_{bb} &= -\frac{1}{4}U_{Ab}^T H_{AA}^{-1} U_{Ab}. \end{aligned} \quad (53)$$

However, the actual calculation of  $F_{\text{eff}}$  is not so easy. Neither  $H_{AA}$  nor  $H_{BB}$  is diagonal, the off-diagonal terms are not in general small, and the higher order harmonics (in  $\mathbf{A}$  and  $\mathbf{B}$ ) are not necessarily unimportant. We will resort to numerical procedures to aid us in finding the eigenvalues and eigenvectors of  $F_{\text{eff}}$ .

If  $r_d^0$  is large then the higher harmonics in  $\mathbf{A}$  and  $\mathbf{B}$  do become less important, and we anticipate that working with finite dimensional  $H_{AA}$ 's and  $H_{BB}$ 's will provide a reasonable approximation to  $F_{\text{eff}}$ . Furthermore, if  $\gamma \neq 0$  then the higher harmonics in  $\mathbf{a}$  and  $\mathbf{b}$  are also rapidly suppressed in  $H_{aa}$  and  $H_{bb}$ , allowing us to work with finite dimensional  $H_{aa}$ 's,  $H_{bb}$ 's and  $U$ 's as well.

Noting that  $\mathbf{a} = (1, \mathbf{0})$  and  $\mathbf{b} = (1, \mathbf{0})$  are the Goldstone modes for  $F_{\text{eff}}$  provides us with one gauge of how well we have approximated  $F_{\text{eff}}$  with finite dimensional matrices. Even if we do include too few modes to correctly identify these Goldstone modes, we will still find bounds on the stability. Including more modes will only make the system more unstable. Fig. 6 shows the stability boundary for  $H_{aa} + Q_{aa}$  and  $H_{bb} + Q_{bb}$  in the  $(A_b, A_s)$  plane. We have used 12 texture modes and 6 shape modes in the numerical calculations. Below are the unstable eigenmodes at the stability boundary for the points indicated in Fig. 6,

- (1)  $\mathbf{a} \approx (0.70, -0.71, 0.01, \mathbf{0})$   
 $\mathbf{b} \approx (0.70, -0.71, 0.01, \mathbf{0})$
- (2)  $\mathbf{a} \approx (0.04, -0.99, 0.01, \mathbf{0})$   
 $\mathbf{b} \approx (0.04, -0.99, 0.01, \mathbf{0})$
- (3)  $\mathbf{a} \approx (0, 1.0, \mathbf{0})$   
 $\mathbf{b} \approx (0, 1.0, \mathbf{0})$
- (4)  $\mathbf{a} \approx (0, 1.0, \mathbf{0})$   
 $\mathbf{b} \approx (0, 1.0, \mathbf{0})$

We see that when  $A_s$  is small the first unstable mode contains significant contributions from the  $n = 1$  mode indicating that the Goldstone modes  $\mathbf{a} = (1, \mathbf{0})$  and  $\mathbf{b} = (1, \mathbf{0})$  have not been properly identified within the numerical approximation. For larger values of  $A_s$  the first unstable modes are pure  $n = 2$  modes and the numerical calculation also correctly identifies the  $n = 1$  modes as zero-eigenvalue mode. Now looking back at the eigenmodes for small  $A_s$  we note that only the  $n = 1$  and  $n = 2$  modes contribute significantly, suggesting that the pure  $n = 2$  mode is always the first mode to go unstable.

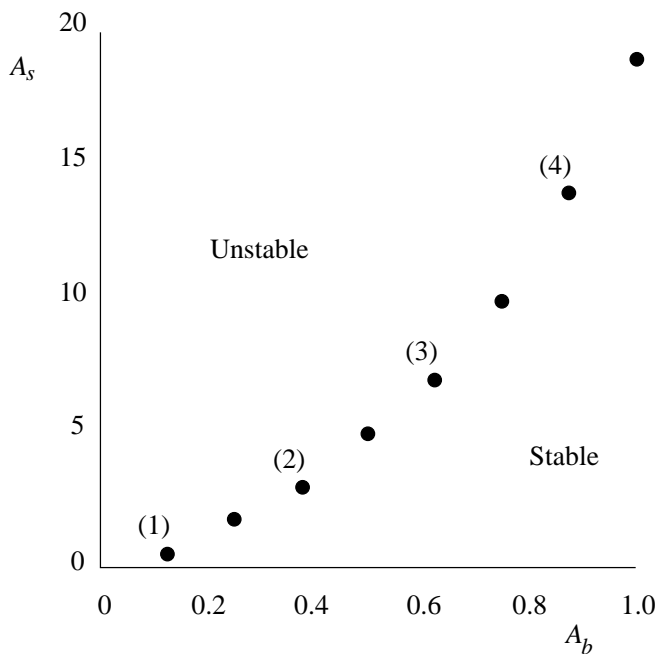


FIG. 6. The stability boundary for  $(H_{aa} + Q_{aa})$  and  $(H_{bb} + Q_{bb})$  as found by using 12 texture and 6 shape modes. The two boundaries are apparently the same within the accuracy of the calculation ( $\approx 10\%$ ). The unstable eigenmodes associated with the noted points are given in the text, one mode each for  $(H_{aa} + Q_{aa})$  and  $(H_{bb} + Q_{bb})$ . Above these points on the boundary the unstable modes appear to be pure  $n = 2$  modes. As noted in the text, it seems likely that the true unstable modes are always the  $n = 2$  modes.

Fig. 6 shows us that for any  $A_s > 0$  there is a critical value of  $A_b$  below which the system becomes unstable. Though not shown in the figure, we remark that as  $A_b$  becomes even smaller, more and more modes become unstable. This should not be surprising since, if  $A_b = 0$  and  $A_s > 0$  then all modes are unstable.

Thus we find that for the free energy (6) the configuration consisting of the disk with the preferred exterior defect texture [(17) with  $\phi_d = 0$  and  $r_d = r_d^0$  (22)] is unstable with respect to correlated changes of the shape and texture when  $A_s > 0$ . Furthermore, the absence of linear terms in  $\mathbf{a}$  and  $\mathbf{b}$  in  $F$  arises from a cancellation between the bulk and boundary portions of the free energy. Hence, changing the structure of either will generically generate such linear terms leading to linear shape instabilities. This helps us understand why either altering the form of the boundary energy or accounting for deviations from the one-coupling-constant approximation also leads to shape instabilities.

## B. The interior defect

Now we will examine the situation with the interior defect. Again, we take  $D$  as in (32) and now we take

$$\Phi_0 = \phi + \frac{\pi}{2}, \quad (55)$$

the preferred texture for a disk as found in section III B. This time, since the defect is inside the disk, it is not possible to make an appropriate choice of the  $P_n$ 's in (36) to change the position of the defect. Nevertheless, we will not allow the defect location to vary. This merely has the effect of removing the Goldstone modes associated with simultaneous translations of the texture and the shape.

We will again work only to quadratic order in  $\boldsymbol{\rho}$  and  $\mathbf{P}$  and extract an effective free energy  $F_{\text{eff}}(\boldsymbol{\rho}, K, \gamma, \mu, R)$ . As with the exterior defect calculation this  $F_{\text{eff}}$  will contain no linear terms in  $\boldsymbol{\rho}$  and the quadratic terms will not always be positive. We will be able to investigate analytically the stability criteria in this case, and we will find again that for any  $A_s > 0$  and for small enough  $A_b$  shape instabilities arise. The answer to the question of which mode becomes unstable first will be much more interesting here. We will find that for the  $k$ th harmonic mode there is always a value of  $A_s$  such that this mode is the first to go unstable as  $A_b$  is lowered from 1. It will always be assumed that  $A_b < 1$  since for larger values we already know from section III B that the defect would prefer to move away from the origin. This will appear in our current analysis as an instability in the  $n = 1$  mode.

As with the exterior defect case, here again it would be necessary to proceed to sixth order in  $\boldsymbol{\rho}$  in the calculation of  $F_{\text{eff}}$  in order to calculate equilibrium shapes. Again this task appears formidable and we will only be examining the stability of the configurations.

Proceeding, we have

$$\begin{aligned}
F = & \pi K \log\left(\frac{R}{\xi}\right) - \pi K \sum_{n \in \mathbb{Z} - \{0\}} \frac{\rho_n \rho_{-n}}{R^2} \\
& + 2\pi K \sum_{n \in \mathbb{Z} - \{0\}} i n P_n R^{|n|} \frac{\rho_{-n}}{R} + 2\pi K \sum_{n=1} n P_n P_{-n} R^{2n} \\
& - 2\pi \mu R + \pi \mu R \sum_{n \in \mathbb{Z} - \{0\}} \frac{\rho_n \rho_{-n}}{R^2} \\
& + \pi \mu R \sum_{n \in \mathbb{Z} - \{0\}} R^{2|n|} P_n P_{-n} \\
& - 2\pi i \mu R \sum_{n \in \mathbb{Z} - \{0\}} n R^{|n|} P_n \frac{\rho_{-n}}{R} \\
& + 2\pi \gamma R + \pi \gamma R \sum_{n \in \mathbb{Z} - \{0\}} (n^2 - 1) \frac{\rho_n \rho_{-n}}{R^2}. \quad (56)
\end{aligned}$$

The absence of any terms linear in  $\mathbf{P}$  with no  $\boldsymbol{\rho}$ 's confirms the extremal nature of the texture. The positive definiteness of the quadratic form associated with the  $\mathbf{P}$ 's confirms that the texture is in fact a minimum with respect to variations that do not change the position of the defect.

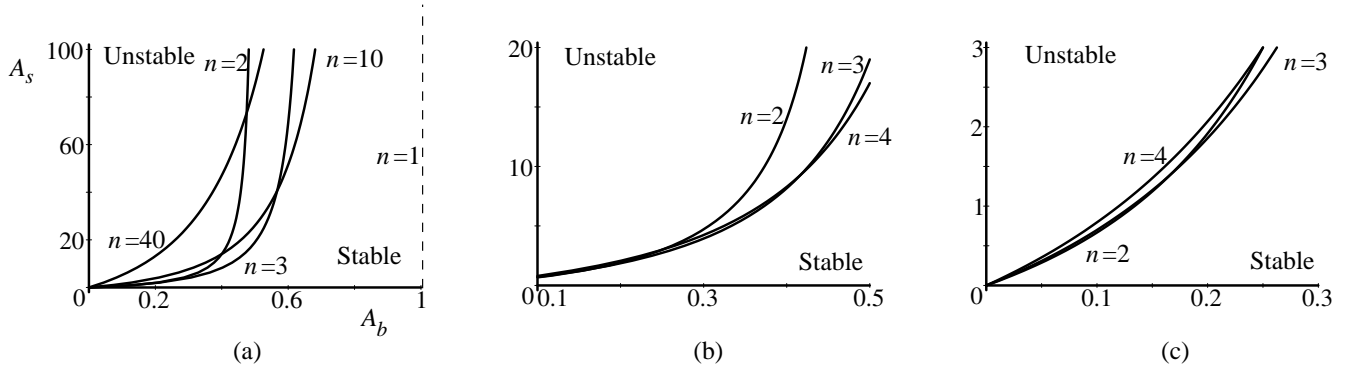


FIG. 7. Stability boundaries in the  $(A_b, A_s)$ -plane for a few modes. Note the  $n = 1$  boundary in (a), this mode is the first to go unstable as  $A_b$  increases beyond 1, instabilities in the other modes for  $A_b > 1$  are not shown. This instability corresponds to the defect wishing to move away from the origin. In all three pictures note the crossing of the stability boundaries. Starting in the stable region, as  $A_b$  is lowered which mode goes unstable first clearly depends upon the value of  $A_s$ . For completeness we note that the  $n$ th stability curve has an asymptote at  $A_b = 1 - 1/n$  as one can see in (a) for the  $n = 2, 3$  curves.

To calculate  $F_{\text{eff}}$  we simply demand that  $\partial F / \partial P_j = 0$  and solve for  $P_j(\rho_n)$ :

$$\begin{aligned} \frac{\partial F}{\partial P_j} = & 2\pi \left( K i j R^{|j|} \frac{\rho_{-j}}{R} + K |j| P_{-j} R^{2|j|} \right) \\ & + 2\pi \left( \mu R R^{2|j|} P_{-j} - \mu i j R R^{|j|} \frac{\rho_{-j}}{R} \right) \end{aligned} \quad (57)$$

$$\text{yields} \quad P_j = i \frac{j}{|j|} \delta_j \frac{1}{R^{|j|}} \frac{\rho_j}{R} \quad (58)$$

$$\text{where} \quad \delta_j = \frac{K - \mu R}{K + \frac{1}{|j|} \mu R}. \quad (59)$$

Substituting into (56) we have

$$\begin{aligned} F_{\text{eff}} = & \pi K \log \left( \frac{R}{\xi} \right) - 2\pi \mu R + 2\pi \gamma R \\ & + 2\pi \mu R \sum_{n=1} \Omega_n \frac{\rho_n \rho_{-n}}{R^2} + O(\rho^3) \end{aligned} \quad (60)$$

where

$$\Omega_n = - \left( A_b - 1 + n \frac{(A_b - 1)^2}{A_b + \frac{1}{n}} - \frac{1}{1 + A_s} (n^2 - 1) \right). \quad (61)$$

Note that to  $O(\rho^2)$   $F_{\text{eff}}$  is block diagonal in the  $\rho_n$ 's and diagonal in the corresponding  $a_n$ 's and  $b_n$ 's. We can examine the stability of the circle simply by looking at the sign of  $\Omega_n$ . If  $\Omega_n$  is negative then the  $n$ th harmonic is unstable.

The stability of the  $n = 1$  mode is independent of  $A_s$  and we can easily see that this mode is unstable when  $A_b > 1$ . This corresponds precisely to our earlier finding (26) that the origin becomes a local maximum for the position of the defect when  $A_b > 1$ .

For the other modes the boundary between the stable and unstable regions in the  $(A_b, A_s)$ -plane is more complex. For the  $n$ th mode this boundary is given by the curve  $\Omega_n = 0$ , or equivalently by,

$$A_s^0(n, A_b) = - \frac{A_b}{1 - A_b} \frac{n^2 + n - 1 - n A_b}{n A_b - n + 1}. \quad (62)$$

We are only interested in the region  $(A_s > -1, 0 < A_b < 1)$ , since physically we require  $(A_b > 0, A_s > -1)$  and we have already seen that the  $n = 1$  mode becomes unstable when  $A_b > 1$ . In Fig. 7 we have plotted  $A_s^0(n, A_b)$  in this region for several values of  $n$ . Within this piece of the  $(A_b, A_s)$ -plane the  $n$ th harmonic mode is stable in the region to the right of  $A_s^0(n, A_b)$  and unstable to the left of this curve.

Fixing the physical elastic constants of the system and allowing the size of the domain ( $R$ ) to change is, in the  $(A_b, A_s)$ -plane, equivalent to fixing  $A_s$  and allowing  $A_b$  to vary. Thus, a growing domain traces out a horizontal line in the  $(A_b, A_s)$ -plane. Starting in the stable region (to the right of the stability curves), as the domain grows which stability boundary the horizontal line crosses first will clearly depend upon the value of  $A_s$ . In fact for

$$\frac{m^4 - 4m^3 + 5m^2 - 4m + 1}{2m - 1} < A_s < \frac{m^4 - m^2 - 2m - 1}{2m + 1} \quad (63)$$

the stability boundary for the  $m$ th harmonic mode will be the first such boundary crossed. Thus the domain will become unstable with respect to  $m$ -fold shape perturbations first. Of course, as the domain grows further it will become unstable with respect to more and more modes. Furthermore there is extensive mode coupling at higher order in  $\rho$ , and as such the equilibrium shape may not exhibit  $m$ -fold shape distortions. Nevertheless, this behavior is markedly different from what we found in the case of the exterior defect. There it appeared that the

$n = 2$  mode always became unstable first. Interestingly, in the extensively investigated dipole model, the  $n = 2$  mode also appears to be the first mode to become unstable. While in both of these cases higher harmonics also become unstable as the domain grows larger, and mode coupling is present, it is still a possibility that  $m$ -fold shape distortions may be more easily accounted for by the present model with a captured defect.

## V. CONCLUSIONS

After a brief review of the relevant types of order present in domains appearing in the coexistence regions of mono-layer films we focused on the effects of the tilt order through the simple  $XY$ -model. We have shown the possible existence of a first-order transition in the texture for a circular domain from a virtual defect texture to a captured defect texture. We then examined the shape instabilities for both of these textures. Through a slightly different parameterization of the domain we were able to reproduce the result of Rudnick and Bruinsma [16] that the circle is an extremum for the virtual defect texture. However, we find that it is not always a minimum and shape instabilities can arise whenever there is the possibility, locally, of a negative effective line tension ( $A_s > 0$ ). For the interior defect texture we have found a complex stability landscape for the fourier modes associated with the domain shape, again arising when  $A_s > 0$ . In both cases larger domains become unstable with respect to the fourier modes. With the exterior defect texture, the  $n = 2$  mode apparently is always the first to become unstable. With the interior defect texture which mode becomes unstable first depends upon the physical parameters of the system.

While the dipole model can also have shape instabilities in its fourier modes, it cannot produce chiral domain shapes. However, for unequal elastic constants the  $XY$ -model may yield chiral shapes. Of course, a general system may have important contributions from the dipole model and from the  $XY$ -model.

## ACKNOWLEDGMENTS

We are grateful for helpful conversations with R. Bruinsma, R. Kamien, and J. Rudnick. This work was supported primarily by the Materials Science and Engineering Center Program of NSF under award DMR96-32598.

## APPENDIX A: SHAPE PARAMETERIZATION

Here we review some of the properties, including advantages and shortcomings, of our choice of parameterization for the boundary of the domain  $D$ . Recall (32)

$$r(\phi) = R_0 + \sum_{n \in \mathbb{Z}^+} (a_n \cos n\phi + b_n \sin n\phi). \quad (\text{A1})$$

Next recall that a domain,  $D$ , is said to be star-shaped if there exists a point  $P_0 \in D$  such that, for all  $P \in D$  the line segment connecting  $P_0$  to  $P$  is contained in  $D$ . The boundary of any star-shaped domain, where the origin can serve as the point  $P_0 \in D$ , can be described by (A1). Correspondingly, a curve given by (A1), if it is also a bounded simple closed curve, serves as the boundary of a star-shaped domain where the origin can be chosen as  $P_0$ .

A priori we have no reason to restrict our attention to star-shaped domains. Unfortunately our parameterization does not allow the description of domains that are not star-shaped and that have boundaries that are simple closed curves (Fig. 8). Furthermore, the parameterization (A1) admits curves that are not simple closed curves and that we would consider to be physically irrelevant (Fig. 8). Thus, if we were to attempt to find highly distorted equilibrium domain shapes, we would be well advised to use a different parameterization.

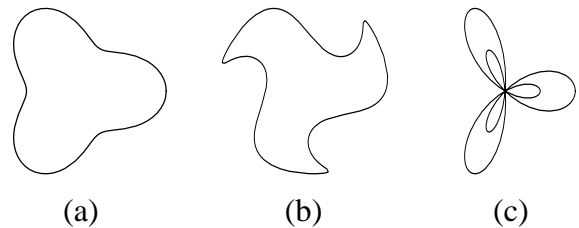


FIG. 8. The simple closed curve in (a) is admitted by the parameterization (A1), it bounds a star-shaped domain. In (b) this simple closed curve does not bound a star-shaped domain and is not admitted by the parameterization (A1). Finally in (c) we have a closed curve with self-intersections which is admitted by (A1).

In this paper, however, we are only interested in investigating the stability of a circular domain. This can be accomplished with the parameterization (A1) since the circular domain is star-shaped and physically relevant infinitesimal perturbations will also be star-shaped.

Another potential difficulty with this parameterization is the special role the origin assumes. Namely, we must be allowed to choose the origin as our special point  $P_0$ . Thus, for example, a circle of radius 1 centered about  $(2, 0)$  cannot be described by the parameterization (A1).

If we are only concerned with the *shape* of the domain, then, if it is star-shaped, we can always choose the origin to be a point in the domain satisfying the properties of  $P_0$ . But now if we are not concerned with the position of the domain with respect to the origin of the coordinate system, then our parameterization contains redundancies. Namely, for each point in the domain that satisfies the required properties of  $P_0$ , we can find a parameterization of the form (A1) which produces the correct boundary. For example, for a disk any interior point could be

chosen as the origin. Translating a domain around in general involves changing all of the Fourier coefficients and so removing this redundancy is not necessarily trivial. However, again, being interested only in small perturbations of a circular domain allows us to easily deal with this redundancy. Starting with a circular boundary centered at the origin,

$$r(\phi) = R, \quad (\text{A2})$$

one finds that for an infinitesimal translation,  $(\epsilon \cos \psi, \epsilon \sin \psi)$ , the translated boundary is given by,

$$r(\phi) = R + (\epsilon \cos \psi) \cos \phi + (\epsilon \sin \psi) \sin \phi + O(\epsilon^2). \quad (\text{A3})$$

That is, to  $O(\epsilon)$  only the  $n = 1$  modes are altered. It is for this reason that one often ignores the  $n = 1$  modes when using this parameterization. To lowest order these modes are merely translations of the domain, and as such merely produce annoying redundancies in the parameterization if one is interested only in the *shape* of the domain. However, in our problems we also have a nontrivial texture present which breaks the isotropy of space. Thus the position of the domain relative to a fixed origin (provided by the texture) is now physically relevant. The redundancies are now in the simultaneous translations of the texture field and the domain.

## APPENDIX B: THE CHOICE OF $\eta = 0$

We would like to comment here on the invariance of our results with respect to our choice of boundary energy, namely  $\eta = 0$  in (6).

Let's consider the two free energies,

$$F_c = \frac{1}{2}K \int_D (\nabla\Phi)^2 d^2x + \eta \oint_{\partial D} \hat{\mathbf{m}} \cdot \hat{\mathbf{n}} ds - \mu \oint_{\partial D} \hat{\mathbf{m}} \cdot \hat{\mathbf{t}} ds + \gamma \oint_{\partial D} ds \quad (\text{B1})$$

and

$$F_a = \frac{1}{2}K \int_D (\nabla\Phi')^2 d^2x + \eta' \oint_{\partial D} \hat{\mathbf{m}}' \cdot \hat{\mathbf{n}} ds + \gamma \oint_{\partial D} ds. \quad (\text{B2})$$

Under the transformation

$$\begin{aligned} \Phi' &= \Phi + \tan^{-1} \frac{\mu}{\eta} \\ \eta' &= \sqrt{\mu^2 + \eta^2} \end{aligned} \quad (\text{B3})$$

we see that  $F_c = F_a$ . Thus, it is trivial to extend our results for  $\eta = 0$  to arbitrary values of  $\eta$  and  $\mu$ .

Interestingly the domain  $D$  does not participate in the transformation. Thus, although  $F_c$  contains a chiral term, indicating that the equilibrium configuration

$(D, \hat{\mathbf{m}})$  should be chiral, we expect  $D$  to be achiral. This follows from the expectation that the equilibrium configuration for  $F_a$ ,  $(D, \hat{\mathbf{m}}')$ , should be achiral since  $F_a$  contains no chiral terms. Thus, the chirality only manifests itself in the equilibrium configuration through the texture  $\hat{\mathbf{m}}$  and not through the shape  $D$ .

- 
- [1] M.M. Lipp, K.Y.C. Lee, J.A. Zasadzinski and A.J. Waring, *Science* **273**, 1196 (1996).
  - [2] G.G. Roberts, in *Langmuir-Blodgett Films*, edited by G.G. Roberts (Plenum Press, New York, 1990), p.317.
  - [3] C.M. Knobler and R.C. Desai, *Ann. Rev. Phys. Chem.* **43**, 207 (1992).
  - [4] H. Mohwald, *Ann. Rev. Phys. Chem.* **41**, 441 (1990).
  - [5] X. Yang, D. Xiao, S. Xiao, Z. Lu and Y. Wei, *Physics Letters A* **193**, 195 (1994).
  - [6] R.M. Weis and H.M. McConnell, *Nature* **310**, 47 (1984).
  - [7] C. Knobler, *Science* **249**, 870 (1990).
  - [8] C.A. Helm and H. Mohwald, *J. Phys. Chem.* **92**, 1262 (1988).
  - [9] R.M. Weis and H.M. McConnell, *J. Phys. Chem.* **89**, 4453 (1985).
  - [10] Q. Xiu, J. Ruiz-Garcia, K.J. Stine, C. Knobler and J. Selinger, *Phys. Rev. Lett.* **67**, 703 (1991).
  - [11] S. Rivière and J. Meunier, *Phys. Rev. Lett.* **74**, 2495 (1995).
  - [12] X. Zhai and M. Kleijn, *Biophysical Journal* **72**, 2651 (1997).
  - [13] Th. Rasing and Y.R. Shen, *Phys. Rev. Lett.* **55**, 2903 (1985).
  - [14] S.W. Hui and H. Yu, *Biophysical Journal* **64**, 150 (1993).
  - [15] G.S. Smith, E.B. Sirota, C.R. Safinya, R.J. Plano and N.A. Clark, *J. Chem. Phys.* **92**, 4519 (1990).
  - [16] J. Rudnick and R. Bruinsma, *Phys. Rev. Lett.* **74**, 2491 (1995).
  - [17] D. Andelman, F. Brochard and J.-F. Joanny, *J. Chem. Phys.* **86**, 3673 (1987).
  - [18] T.K. Vanderlick and H. Mohwald, *J. Phys. Chem.* **94**, 886 (1990).
  - [19] H.M. McConnell, *J. Phys. Chem.* **94**, 4728 (1990).
  - [20] R. de Koker and H.M. McConnell, *J. Phys. Chem.* **97**, 13419 (1993).
  - [21] S.A. Langer, R.E. Goldstein and D.P. Jackson, *Phys. Rev. A* **46**, 4894 (1992).
  - [22] M. Seul, *J. Phys. Chem.* **97**, 2941 (1993).
  - [23] K.Y.C. Lee and H.M. McConnell, *Biophysical Journal* **68**, 1740 (1995).
  - [24] H.M. McConnell and V.T. Moy, *J. Phys. Chem.* **92**, 4520 (1988).
  - [25] J. Fang, E. Teer, C.M. Knobler, K. Loh and J. Rudnick, *Phys. Rev. E* **56**, 1859 (1997).
  - [26] I. Kraus, XVII *International Liq. Cryst. Conf.* (1998).
  - [27] P. Chaikin and T.C. Lubensky, *Principles of Condensed Matter Physics* (Cambridge University Press, Cambridge, 1995).

- [28] S.A. Langer and J.P. Sethna, Phys. Rev. A **34**, 5035 (1986).
- [29] In general, there will be an additional term in chiral systems:  $K_{sb}(\nabla \cdot \hat{\mathbf{m}})(\nabla \times \hat{\mathbf{m}})$ .
- [30] S. Dierker, R. Pindak and R.B. Meyer, Phys. Rev. Lett. **56**, 1819 (1986).
- [31] J. Selinger and D. Nelson, Phys. Rev. A **39**, 3135 (1989).
- [32] D. Pettey and T.C. Lubensky, J. Phys. II France **3**, 1571 (1993).